

1 **Influence of the Amazon River on the Nd isotope composition of
2 deep water in the western equatorial Atlantic during the Oligocene-
3 Miocene transition**

4 Joseph A. Stewart ^{a,b*}, Marcus Gutjahr ^c, Rachael H. James ^a, Pallavi Anand ^d, Paul A. Wilson ^a

5 ^a National Oceanography Centre Southampton, University of Southampton, European Way, Southampton, SO14
6 3ZH, UK.

7 ^b National Institute of Standards and Technology, Hollings Marine Laboratory, 331 Fort Johnson Rd, Charleston,
8 SC, 29412, USA

9 ^c GEOMAR Helmholtz Centre for Ocean Research Kiel, Wischhofstraße 1-3 D-24148 Kiel, Germany

10 ^d School of Environment, Earth and Ecosystem Science, Walton Hall, The Open University, Milton Keynes, MK7
11 6AA, UK

12 *Corresponding author. Tel: +1 843 725 4833, Email: Joseph.Stewart@noaa.gov

14 Abstract:

15 Dissolved and particulate neodymium (Nd) are mainly supplied to the oceans via
16 rivers, dust, and release from marine sediments along continental margins. This
17 process, together with the short oceanic residence time of Nd, gives rise to
18 pronounced spatial gradients in oceanic $^{143}\text{Nd}/^{144}\text{Nd}$ ratios (ϵ_{Nd}). However, we do not
19 yet have a good understanding of the extent to which the influence of riverine point-
20 source Nd supply can be distinguished from changes in mixing between different
21 water masses in the marine geological record. This gap in knowledge is important to
22 fill because there is growing awareness that major global climate transitions may be
23 associated not only with changes in large-scale ocean water mass mixing, but also
24 with important changes in continental hydroclimate and weathering. Here we present
25 ϵ_{Nd} data for fossilised fish teeth, planktonic foraminifera, and the Fe-Mn
26 oxyhydroxide and detrital fractions of sediments recovered from Ocean Drilling
27 Project (ODP) Site 926 on Ceara Rise, situated approximately 800 km from the
28 mouth of the River Amazon. Our records span the Mi-1 glaciation event during the
29 Oligocene-Miocene transition (OMT; ~23 Ma). We compare our ϵ_{Nd} records with
30 data for ambient deep Atlantic northern and southern component waters to assess the
31 influence of particulate input from the Amazon River on Nd in ancient deep waters at
32 this site. ϵ_{Nd} values for all of our fish teeth, foraminifera, and Fe-Mn oxyhydroxide
33 samples are extremely unradiogenic ($\epsilon_{\text{Nd}} \approx -15$); much lower than the ϵ_{Nd} for deep
34 waters of modern or Oligocene-Miocene age from the North Atlantic ($\epsilon_{\text{Nd}} \approx -10$) and

35 South Atlantic ($\varepsilon_{\text{Nd}} \approx -8$). This finding suggests that partial dissolution of detrital
36 particulate material from the Amazon ($\varepsilon_{\text{Nd}} \approx -18$) strongly influences the ε_{Nd} values
37 of deep waters at Ceara Rise across the OMT. We conclude that terrestrially derived
38 inputs of Nd can affect ε_{Nd} values of deep water many hundreds of kilometres from
39 source. Our results both underscore the need for care in reconstructing changes in
40 large-scale oceanic water-mass mixing using sites proximal to major rivers, and
41 highlight the potential of these marine archives for tracing changes in continental
42 hydroclimate and weathering.

43 Keywords: Neodymium isotopes, fish teeth, foraminifera, Amazon, Oligocene-Miocene, ODP Site 926

44 1 Introduction

45 The weathering and transport of continental rock substrate is a major source of
46 dissolved neodymium to the oceans (Goldstein and Jacobsen, 1987). The neodymium
47 isotopic composition ($\varepsilon_{\text{Nd}} = [({}^{143}\text{Nd}_{\text{sample}} / {}^{144}\text{Nd}_{\text{sample}}) / ({}^{143}\text{Nd}_{\text{CHUR}} / {}^{144}\text{Nd}_{\text{CHUR}}) - 1] \times$
48 10^4 ; where CHUR is the chondritic uniform reservoir) of continental rocks varies
49 according to both the Sm/Nd ratio and age of the rock, such that ancient continental
50 crust exhibits very low (unradiogenic) ε_{Nd} values (down to -40), whereas younger
51 volcanic sequences generally have much higher (radiogenic) values (up to $+12$;
52 Goldstein and Hemming, 2003). Because neodymium has a residence time on the
53 order of the mixing time of the ocean (500 to 2000 yr; Piepgras and Wasserburg,
54 1987; Tachikawa et al., 2003), deep waters formed in the North Atlantic, which is
55 surrounded by Proterozoic and Archean rocks, are characterised by low ε_{Nd} (-13.5 ;
56 Piepgras and Wasserburg, 1987; Lacan and Jeandel, 2005a). On the other hand, deep
57 water masses formed in the Southern Ocean have higher ε_{Nd} (between -7 and -9 ;
58 Piepgras and Wasserburg, 1987; Jeandel, 1993; Stichel et al., 2012) due to the
59 contribution of young mantle-derived material surrounding the Pacific Ocean that
60 mixes with Atlantic waters in this region. Records of seawater ε_{Nd} values recorded in
61 marine sediments have therefore been widely used to identify the source of the
62 overlying water masses (Scher and Martin, 2004; Piotrowski et al., 2005).

In addition to the influence of riverine solute inputs, the isotopic composition of dissolved Nd in seawater can be modified by exchange of Nd in river-born particulate material with seawater via “boundary exchange” on continental margins (Jeandel et al., 2007; Pearce et al., 2013) and also in certain deep sea settings (Lacan and Jeandel, 2005b; Carter et al., 2012; Wilson et al., 2012; Abbott et al., 2015b). Various modelling studies even suggest that release of Nd from continental margins is by far the dominant source of Nd to the oceans (contributing as much as 90%; Arsouze et al., 2009; Rempfer et al., 2011). Dissolved deep water ε_{Nd} at these continental margin locations is likely a function of three variables: (i) the magnitude of the Nd flux from sediment pore fluids, (ii) the difference between the ε_{Nd} value of the overlying water and the pore fluid, and (iii) the exposure time to this benthic flux of Nd (Abbott et al., 2015a).

The Amazon River is the world’s largest river and each year carries 5×10^8 tons of suspended sediment (Gibbs, 1967) that is relatively enriched in Nd (~ 40 ppm; McDaniel et al., 1997) compared to seawater (typically <10 ppb; Piepraga and Wasserburg, 1987). These Nd-rich Amazon sediments have been shown to influence the dissolved ε_{Nd} of near-shore seawater (e.g. the mid-salinity zone of the Amazon Estuary; Rousseau et al., 2015), and have also been suggested to affect deep water ε_{Nd} as far afield as the Caribbean Sea (Osborne et al., 2014). An improved understanding of the extent to which river-born particulate material can influence deep water ε_{Nd} is, therefore, critical to our understanding of Nd cycling in the oceans (Stichel et al., 2012; Kraft et al., 2013; Pearce et al., 2013). This is particularly true for major climate transitions when rock weathering and the flux of riverine particulate material may vary (West et al., 2005), centres of precipitation can shift altering river drainage patterns (Wang et al., 2004), and ocean circulation can change the exposure time of water masses to benthic sources of Nd (Abbott et al., 2015a). Records of past seawater and associated sediment ε_{Nd} in relative proximity to major riverine sources of Nd such as the Amazon River are therefore vital to understanding Nd exchange between particulate and dissolved phases in continental margin settings.

92 1.1 Archives of seawater ε_{Nd}

93 Fossilised fish teeth recovered from deep sea sediment cores are an ideal substrate for
94 reconstructing past changes in ε_{Nd} values of ancient bottom waters. Fish teeth are
95 found throughout the world's oceans and incorporate the majority of their Nd post-
96 mortem (>100 ppm Nd), during early diagenetic recrystallization of the biogenic
97 apatite at the sediment-seawater interface. They are therefore resistant to late
98 diagenetic overprinting (Martin and Scher, 2004). Analysis of Nd associated with
99 authigenic Fe-Mn oxyhydroxides in marine sediments can also be used to extract
100 bottom water Nd isotope compositions (Piotrowski et al., 2005), although care must
101 be taken during sample processing (Elmore et al., 2011).

102 The only method by which ε_{Nd} values of surface waters have been successfully
103 reconstructed to date is through the analysis of reductively cleaned planktonic
104 foraminifera (Vance and Burton, 1999). However, because diagenetic
105 ferromanganese coatings formed on the seafloor and in pore waters are extremely
106 enriched in Nd (200 ppm) compared with biogenic calcite (0.1 ppm), these coatings
107 must be effectively removed (Pomiès et al., 2002). ε_{Nd} records of cleaned planktonic
108 foraminifera that have elevated Nd/Ca are likely compromised by incomplete
109 removal (<98%) of ferromanganese coatings or reabsorption of Nd released during
110 the cleaning process. For this reason, even cleaned foraminifera often exhibit ε_{Nd}
111 values similar to bottom waters (Roberts et al., 2012; Tachikawa et al., 2014).

112 1.2 Scope of this study

113 Here we assess evidence for changes in continental inputs from the Amazon River
114 during the Oligocene-Miocene transition (OMT), through analysis of ε_{Nd} in fish teeth,
115 planktonic foraminifera, and the Fe-Mn oxyhydroxide and detrital fractions of
116 sediments recovered from ODP Site 926 (Figure 1). The OMT is marked by a
117 positive excursion (>1‰) in benthic foraminiferal $\delta^{18}\text{O}$ at 23 Ma (Figure 2) that
118 represents cooler deep-water temperatures and increased Antarctic ice volume
119 associated with the so-called Mi-1 glaciation event (Pälike et al., 2006; Liebrand et
120 al., 2011). We use our ε_{Nd} data to assess the contribution of the Amazon as a source

121 of Nd to the regional Equatorial Atlantic water mass signal at this site during this
122 interval of climatic variability, and discuss the implications of these data for
123 interpretation of ε_{Nd} records in terms of water mass mixing.

124 **2 Materials and methods**

125 **2.1 Geological setting and core chronology**

126 Samples spanning the OMT were selected from sediment cores recovered from ODP
127 Leg 154, Site 926, Hole B ($3^{\circ}43.148'\text{N}$, $42^{\circ}54.507'\text{W}$, ~3600 m water depth; Leg 154
128 Shipboard Scientific Party, 1995), situated approximately 800 km to the northeast of
129 the mouth of the River Amazon (Figure 1). The geographic position and water-depth
130 of Site 926 have not changed significantly since the Oligocene. Although there is no
131 magnetostratigraphic age control available for ODP Leg 154 cores, a high quality
132 orbital chronology is available for the Oligocene-Miocene sequence at ODP Site 926
133 (Pälike et al., 2006) and can be correlated to ODP Site 1090 on the Agulhas Ridge
134 (Liebrand et al., 2011) where a high quality magnetostratigraphy is available (Figure
135 2; Channell et al., 2003). We apply the age model of Pälike et al. (2006).

136 **2.2 Sample preparation**

137 Sediment samples were dried in an oven at 50°C , then gently disaggregated in
138 deionised water using a shaker table and washed over a $63 \mu\text{m}$ sieve. Tests (~1 mg) of
139 the planktonic foraminifer *Dentoglobigerina venezuelana* were picked from the 355-
140 $400 \mu\text{m}$ size fraction for trace element analysis (See Supplementary Information)
141 following the morphotype description of Stewart et al., (2012). Larger samples of *D.*
142 *venezuelana* (~25 mg) and a second species, *Globigerina bulloides* (~5 mg), were
143 picked for Nd isotope analysis from the $>355 \mu\text{m}$ size fraction. Additionally,
144 fossilised fish teeth (and one fish bone sample) were taken for ε_{Nd} analysis. These
145 samples consisted of an average of three individual teeth.

146 *2.2.1 Detrital and authigenic Fe-Mn oxyhydroxide extraction*

147 Dried and ground bulk sediment (~420-610 mg) was transferred into centrifuge tubes
148 for processing. After an initial wash in MQ water and centrifuging, 15 ml of a
149 reductive cocktail containing 0.05 M hydroxylamine hydrochloride, 15% acetic acid,
150 and 0.01 M buffered EDTA was added following methods of Blaser et al. (2016),
151 with reductive cocktail concentrations as used in Gutjahr et al. (2007). Samples were
152 centrifuged and the supernatant was removed for purification of Nd from the Fe-Mn
153 oxyhydroxide fraction. Another 25 ml of the reductive leaching solution was added to
154 remove any remaining Fe-Mn oxyhydroxides (Gutjahr et al., 2007) in order to target
155 the pure terrigenous signal without residual authigenic Nd contributions. After
156 shaking for 24 hours, the supernatant was discarded following centrifuging and the
157 sample was dried. Approximately 50 mg of the dried re-homogenised residue was
158 first treated with concentrated HNO₃ and 30% H₂O₂ for effective oxidation of
159 organics. Dried samples were subsequently treated with aqua regia prior to pressure
160 digestion in steel bombs (190°C over three days) in a mixture of concentrated HNO₃
161 and HF. Dried digested samples were treated three times with concentrated HNO₃
162 before conversion to chloride with HCl and column purification using procedures
163 outlined in Section 2.2.3.

164 *2.2.2 Foraminifera and fish tooth cleaning procedure*

165 All foraminifera and fish teeth samples were subject to cleaning prior to analysis
166 using established methods (Rosenthal et al., 1999). Briefly, adhering clay particles
167 were removed through repeated ultrasonication and rinsing with MQ water and
168 methanol. Samples were then cleaned to remove ferromanganese oxide coatings and
169 organic matter, and finally leached in weak acid to remove any re-adsorbed ions.
170 Foraminiferal calcite and fish teeth samples for isotopic analysis were dissolved in
171 0.075 M and 0.15 M HNO₃ respectively.

172 *2.2.3 Separation of Nd from the sample matrix*

173 Nd was separated from the sample matrix using a two-stage chromatography
174 procedure. Sample solutions were dried down on a hotplate and then re-dissolved in

175 0.2 M HCl. This solution was then loaded onto a Teflon column containing 2.4 ml of
176 Bio-Rad™ AG50W-X12 cation exchange resin. Matrix elements were removed by
177 eluting with 4 M HCl. Rare earth elements were then collected in 6 M HCl. The
178 recovered rare earth fraction was dried down, re-dissolved in 0.18 M HCl, and loaded
179 onto a second cation exchange column containing 0.6 ml of Eichron™ Ln spec resin
180 of particle size 50 to 100 µm. Residual Sr and approximately 90% of the Ce were first
181 eluted with 8 ml of 0.18 M HCl, and the Nd fraction was collected by addition of a
182 further 7 ml of 0.18 M HCl. The total procedural blank from the columns was 13 pg
183 of Nd, which is typically <<1% of the sample size.

184 2.3 Analytical techniques

185 Details and results of analysis of Nd/Ca and Mn/Ca in foraminiferal calcite are shown
186 in the Supplementary Information. The Nd isotopic composition of the fish teeth and
187 foraminifera was determined by multicollector inductively coupled plasma mass
188 spectrometry (MC-ICP-MS; ThermoFisher Neptune) at the University of
189 Southampton, and the Nd isotopic composition of the sediment leaches and digests
190 was carried out at GEOMAR in Kiel (MC-ICP-MS; ThermoFisher Neptune Plus),
191 using the method of Vance and Thirwall (2002). Measured $^{143}\text{Nd}/^{144}\text{Nd}$ ratios were
192 corrected to a $^{146}\text{Nd}/^{144}\text{Nd}$ ratio of 0.7219 to remove mass bias effects (Wombacher
193 and Rehkämper, 2003). The external reproducibility of our Nd isotope measurements,
194 for Nd solutions of 25 to 50 ppb is better than ± 0.16 ($n=37$) and ± 0.11 ($n=19$) ε units
195 (2σ) in Southampton and Kiel, respectively. Corrected data were normalised by
196 adjusting the average $^{143}\text{Nd}/^{144}\text{Nd}$ ratio of the JNd-1 Nd isotope standard measured
197 during that analytical session to the accepted value of 0.512115 (Tanaka et al., 2000).
198 $^{143}\text{Nd}/^{144}\text{Nd}$ ratios ($\varepsilon_{\text{Nd}(0)}$) were corrected for post-depositional ingrowth of ^{143}Nd
199 from ^{147}Sm ($\varepsilon_{\text{Nd}(t)}$) using an initial $^{147}\text{Sm}/^{144}\text{Nd}$ ratio of 0.1286 for fish teeth (Thomas
200 et al., 2003) and 0.1412 for foraminifera, detrital and Fe-Mn oxyhydroxide samples
201 (Vance et al., 2004). This adjustment is small for our samples (lowering ε_{Nd} by <0.17
202 units). All subsequent discussion refers to the adjusted $\varepsilon_{\text{Nd}(t)}$ values.

204 3 Results

205 In Figure 2 we compare our records of ε_{Nd} in the detrital fraction, Fe-Mn
206 oxyhydroxides (Table 1), fish teeth, and foraminifera (*D. venezuelana*, and *G.*
207 *bulloides*; Table 2) from ODP Site 926 with the benthic foraminiferal oxygen isotope
208 record from the same site (Figure 2 A; Pälike et al., 2006). We further compare these
209 ε_{Nd} measurements to records of representative contemporaneous deep water ε_{Nd}
210 (Figure 1; Figure 2 B) from the North (Fe-Mn crust ALV539; O'Nions et al., 1998),
211 South (fish teeth from ODP Site 1090; Scher and Martin, 2008), and Equatorial
212 Atlantic Ocean (Fe-Mn crust ROM46; Frank et al., 2003). With the exception of the
213 North Atlantic Fe-Mn crust site ALV539 (depth 2.7 km) the water depths (and
214 palaeodepths) of all of these sites are similar to that of Ceara Rise (Figure 1). Despite
215 its slightly shallower depth, we assume that the ε_{Nd} of seawater at Site ALV539 is
216 typical of northern sourced deep water to Ceara Rise.

217 Most of our data for the detrital fraction from the OMT at Ceara Rise show distinctly
218 unradiogenic ε_{Nd} values with a baseline of around -18ε units. Four samples show
219 slightly more radiogenic values (around -16.5ε units) at 22.4, 23.3, 23.6, and 24.1
220 Ma but the occurrence of these data points shows no clear correspondence to
221 structure in the benthic foraminiferal oxygen isotope stratigraphy from the same site.

222 ε_{Nd} values for fish teeth are, on average, -14.5 and all data points are lower than
223 -13.0ε units. The foraminiferal ε_{Nd} records for *D. venezuelana* and *G. bulloides* are
224 generally within analytical uncertainty of one another and vary between -16.5 and $-$
225 13.2ε units. Compositions of the Fe-Mn oxyhydroxide fraction are within 0.26ε
226 units of the foraminiferal ε_{Nd} values. Furthermore, the pattern of change seen in the
227 Fe-Mn oxyhydroxide and foraminiferal ε_{Nd} records is remarkably similar to that of
228 the fish teeth record. We therefore find no discernible difference between the fish
229 teeth, foraminifera, and Fe-Mn oxyhydroxide ε_{Nd} records, even during the large
230 oxygen isotope excursion corresponding to the Mi-1 glaciation event.

231 4 Discussion

232 To assess the potential influence of input of riverine particulate material from the
233 Amazon to Ceara Rise, we first discuss the Nd isotope composition of the detrital
234 fraction of the sediments. We then assess the impact of the Amazon on the Nd
235 isotopic composition of seawater in the western equatorial Atlantic across the OMT
236 by comparing Nd isotope compositions in the three different palaeo-seawater
237 substrates.

238 4.1 Source of detrital sediments at Ceara Rise

239 The Nd isotopic composition of the detrital fraction of the sediments is used to assess
240 the Nd isotopic signature of terrestrial material from the Amazon River reaching the
241 Ceara Rise during the OMT. Sediment particles delivered to the modern Amazon Fan
242 from the River Amazon and its tributaries exhibit a wide range of ϵ_{Nd} values today
243 (from -8 to -22 ; Allègre et al., 1996), reflecting the variable age of the catchment
244 bedrock (Figure 3 A). Unradiogenic ϵ_{Nd} values are observed in the eastern tributaries
245 (Tapajós tributary $\epsilon_{\text{Nd}} = -20$, Trombetas tributary $\epsilon_{\text{Nd}} = -22$; Allègre et al., 1996),
246 which drain ancient cratonic sequences of the Guiana Shield (>2.3 Ga). By contrast,
247 the western tributaries draining younger Phanerozoic sedimentary rocks have more
248 radiogenic sedimentary particulate loads ($\epsilon_{\text{Nd}} \sim -8$). These eroded sediments from the
249 east and west tributaries combine to give an intermediate ϵ_{Nd} value for the modern
250 Amazon suspended sediment load output to the Atlantic Ocean, which has $\epsilon_{\text{Nd}} = -10$
251 (Allègre et al., 1996; McDaniel et al., 1997; Rousseau et al., 2015). These large
252 regional distinctions in ϵ_{Nd} composition between geological terranes mean that
253 changes in drainage patterns have the potential to give rise to dramatic changes in the
254 ϵ_{Nd} of riverine suspended sediments to the Atlantic Ocean.

255 The drainage of the Amazon during the Oligocene and Miocene is thought to have
256 been very different from today because of the lower altitude of the Andes (Figure 3
257 B; Campbell et al., 2006; Figueiredo et al., 2009; Shephard et al., 2010). Stratigraphic
258 records suggest that, prior to the middle-Miocene (Cunha et al., 1994; Eiras et al.,
259 1994), the Amazon Basin consisted of two catchments divided by the Purus Arch: the
260 Eastern Amazon basin to the east and the Pebas Wetlands to the west (Figueiredo et

261 al., 2009). Under this configuration, the outflow from the Amazon to the Atlantic
262 would have originated almost exclusively from the Eastern Amazon Basin, which is
263 underlain by the Guiana Shield and today yields very unradiogenic ε_{Nd} values for
264 suspended loads, between -17 and -22 (Allègre et al., 1996). The low ε_{Nd} values
265 recorded in the detrital fraction (-18ε units) that we document at Site 926, together
266 with colour, grain-size and rare earth element logs of sediments recovered from other
267 ODP Leg 154 sites (Dobson et al., 2001), all suggest that the Guiana Shield was the
268 dominant source of terrigenous sediment to Ceara Rise throughout our study interval.

269 Four samples in our data set show higher ε_{Nd} in the detrital fraction (up to -16.5) and
270 are interpreted to reflect the incorporation of detrital material from more radiogenic
271 terranes adjacent to the ancient Guiana Shield. One possible source of more
272 radiogenic Nd is the westerly Purus Arch (Figure 3 B). Changes in Amazon
273 vegetation cover (e.g. van der Hammen and Hooghiemstra, 2000) and distribution of
274 precipitation have been linked to global climate (Wang et al., 2004), as centres of
275 tropical precipitation are often shifted meridionally away from the hemisphere of
276 maximum cooling (Arbuszewski et al., 2013). Nearly all detrital ε_{Nd} values are
277 slightly higher (more radiogenic) before the Mi-1 event than they are afterwards, but
278 there is no obvious relationship between our detrital ε_{Nd} record and the benthic $\delta^{18}\text{O}$
279 record across the OMT (Figure 2 A; Pälike et al., 2006), even during the Mi-1
280 glaciation. We therefore conclude that changes in the source of Amazonian
281 terrigenous sediment to Site 926 during our study interval are not strongly modulated
282 by processes coupled to changes in high latitude temperature and continental ice
283 volume. On the other hand, our data indicate that measurement of detrital ε_{Nd} of more
284 recent Ceara Rise sediments (e.g. McDaniel et al., 1997) could represent a powerful
285 tool for determining the disputed timing of westward enlargement of the Amazon
286 Basin to its modern configuration during the Miocene/Pliocene (Campbell et al.,
287 2006; Figueiredo et al., 2009).

288 4.2 Nd in fish teeth and fossilised foraminifera at Ceara Rise

289 Of the data types presented here, those generated using fish teeth are commonly
290 regarded as the most robust archive of changes in oceanic bottom water ε_{Nd} because
291 most of the Nd contained in fish tooth fluorapatite is acquired during early diagenesis
292 on the seafloor (Martin and Haley, 2000; Martin and Scher, 2004). In our study, ε_{Nd}
293 data from planktonic foraminifera are strikingly similar to data from fish teeth and the
294 authigenic Fe-Mn oxyhydroxide fraction, despite reductive cleaning that is expected
295 to remove authigenic overgrowths from test calcite. While it is possible that the ε_{Nd}
296 value of surface water was identical to the ε_{Nd} value of bottom water during the
297 OMT, high Mn/Ca ($>500 \mu\text{mol/mol}$) and Nd/Ca ($>1 \mu\text{mol/mol}$) ratios measured in
298 these foraminifera (see Supplementary Information) imply that the Nd in these
299 samples more likely has an authigenic origin and is not representative of surface
300 water (Pomiès et al., 2002; Tachikawa et al., 2014).

301 4.3 Sources of Nd to deep water at Ceara Rise

302 Fish teeth ε_{Nd} records from South Atlantic ODP Sites 689, Maud Rise (Scher and
303 Martin, 2004) and 1090, Agulhas Ridge (Scher and Martin, 2006; Figure 2 B) suggest
304 that, during the OMT, Atlantic deep waters originating in the Southern Ocean had ε_{Nd}
305 values close to those of modern southern component water ($\varepsilon_{\text{Nd}} \sim -8$). Unradiogenic
306 ε_{Nd} values typical of modern northern component deep water (-13.5 ; principally
307 North Atlantic Deep Water; Piegras and Wasserburg, 1987; Lacan and Jeandel,
308 2005a) only appear in the marine sedimentary record in the late Neogene, following
309 closure of the Central American Seaway (Burton et al., 1997). The ε_{Nd} value of
310 northern component deep water in the Miocene is estimated to have been much
311 higher (~ -10 ; O'Nions et al., 1998; Scher and Martin, 2006) than its present day
312 composition. Thus, simple mixing between northern and southern component deep
313 waters cannot explain the low ε_{Nd} that we document in fish teeth, planktonic
314 foraminifera, and the authigenic Fe-Mn fraction of sediments from Site 926 (~ -15
315 ε_{Nd} units; Figure 2 B). Rather, the deep waters must be affected by input of very
316 unradiogenic Nd from a regional source, a clear candidate being the River Amazon.

317 Neodymium is exported from rivers to the oceans in three main phases, (i) dissolved
318 Nd (Goldstein and Jacobsen, 1987), (ii) pre-formed oxides (Bayon et al., 2004), and
319 (iii) Nd contained in detrital suspended particulate matter (Pearce et al., 2013).
320 Various lines of evidence point to detrital particulate-bound supply as the major
321 influence on deep water ϵ_{Nd} at Ceara Rise. First, dissolved Nd concentration in the
322 modern Amazon Estuary is observed to increase in the mid-salinity zone and is
323 accompanied by a shift in ϵ_{Nd} from riverine values (>-9) to values closer to the
324 suspended load (<-10) (Rousseau et al., 2015). Therefore, Nd in the dissolved phase
325 of Amazon river waters is extremely susceptible to alteration by Nd released from
326 suspended particles during estuarine mixing. Second, if pre-formed Fe-Mn oxides
327 were controlling the bottom water Nd isotope signature at Ceara Rise, this should be
328 most clearly identifiable in isotopic differences between fish tooth- and Fe-Mn
329 oxyhydroxide-derived ϵ_{Nd} . In such a scenario, the Fe-Mn oxyhydroxides would yield
330 ϵ_{Nd} values similar to the detrital composition (*c.f.* Bayon et al., 2004; Kraft et al.,
331 2013). By contrast, the Nd incorporated into fish teeth is derived from bottom waters
332 or pore fluids (Martin and Scher, 2004). Hence, our data indicate that pore fluid and
333 bottom water ϵ_{Nd} at Ceara Rise differed from that of deep water in the central Atlantic
334 (with $\epsilon_{\text{Nd}} \sim -10$; O'Nions et al., 1998). The most likely reason for this is partial
335 dissolution of Amazon particulate material within Ceara Rise pore fluids (Lacan and
336 Jeandel, 2005a; Carter et al., 2012; Pearce et al., 2013; Abbott et al., 2015a). Once
337 delivered to Ceara Rise, this particulate-bound Nd is transferred to the overlying deep
338 waters through dissolution or desorption, thus shifting the deep water signal
339 regionally towards less radiogenic ϵ_{Nd} values. Discovery of this signal at a site more
340 than 800 km from the outflow source, in 3.6 km water depth, indicates that this
341 process is not restricted to the continental shelves and can operate further offshore if
342 particle fluxes are high.

343 To assess the percentage contribution of detrital Amazon-derived Nd to deep water
344 ϵ_{Nd} at this site we compare fish tooth, foraminifera, and Fe-Mn oxyhydroxide data,
345 with ϵ_{Nd} measurements of the corresponding detrital fraction and open ocean
346 seawater. In this analysis, we used the detrital measurement closest to the sample

347 depth of the fish tooth, foraminifera and leachate data where data from the same
348 sample was not available (we note that our choice between detrital data from identical
349 or adjacent samples for comparison to estimates of seawater ε_{Nd} has little impact on
350 the main findings of this study). Assuming that the ε_{Nd} value of northern component
351 water bathing Ceara Rise during the OMT was -10 (O'Nions et al., 1998), we
352 calculate that the majority of the Nd in bottom waters at this site (average 64%) was
353 derived from Amazon particulate material (Figure 2 C). Although we observe large
354 amplitude variability in our down-core record (between 45% and 90%) that is likely
355 related to variations in sediment sourcing from various Amazon tributaries (Figure 3),
356 there is no clear link between short-term increases/decreases in the estimated fraction
357 of Amazon particulate-derived Nd on the ε_{Nd} signal of Ceara Rise bottom water and
358 pronounced changes in high latitude climate inferred from benthic foraminiferal $\delta^{18}\text{O}$
359 (Figure 2 A; Pälike et al., 2006).

360 We note that ε_{Nd} values for deep water of similar age and water depth to our samples
361 derived from a Fe-Mn crust (ROM46) recovered from the central Equatorial Atlantic
362 Ocean are also relatively unradiogenic (-11.5 ; Figure 2 B), and also cannot therefore
363 be explained by simple mixing between northern and southern component deep
364 waters (Frank et al., 2003). Such unradiogenic deep water ε_{Nd} at the ROM46 site,
365 more than 1,000 km from land, prompted the authors to invoke additional sources of
366 Nd including Saharan dust and also the Amazon River (Frank et al., 2003). Our new
367 data from Ceara Rise support a far-reaching Amazon source for deep water Nd at the
368 ROM46 site during the Oligocene-Miocene, given that this more distal central
369 Atlantic site yields deep water ε_{Nd} values that fall between those observed at Ceara
370 Rise and contemporaneous northern/southern component water.

371 4.4 Potential impact of regional terrestrial inputs on seawater ε_{Nd} in the Neogene
372 Ocean

373 The highly unradiogenic ε_{Nd} composition of suspended particulate material in the
374 Amazon River during the OMT points to more restricted drainage than in the
375 Amazon Basin today, with the dominant terrestrial input coming from the ancient

376 terrane of the Guiana Shield in the East Amazon Basin. The fingerprint of this highly
377 unradiogenic sediment source on deep water ε_{Nd} is recognisable far from the Amazon
378 outflow source, yielding values outside of the range defined by mixing of northern
379 and southern component water masses in the Atlantic. This result is consistent with
380 the findings of Abbott et al. (2015a), who suggest that seawater ε_{Nd} can be strongly
381 affected by inputs of pore fluid Nd if the ε_{Nd} of those pore fluids is significantly offset
382 from that of the overlying water mass.

383 In more recent geological times the flux and ε_{Nd} composition of the open deep
384 Equatorial Atlantic water mass and Amazon weathering sources have changed. First,
385 the sediment flux from the Amazon increased from the late Miocene to the Pliocene
386 in conjunction with Andean uplift (Figueiredo et al., 2009). This uplift has also
387 resulted in a larger modern Amazon drainage basin that now includes younger
388 Phanerozoic sedimentary rocks (Figueiredo et al., 2009). As the ε_{Nd} of suspended
389 sediments is strongly influenced by drainage pattern changes in the heterogeneous
390 Amazon basin, broadening of the Amazon catchment westwards introduces
391 suspended sediments with more radiogenic compositions ($\varepsilon_{\text{Nd}} \sim -10$; Figure 3 A;
392 Allègre et al., 1996; Rousseau et al., 2015). Second, the ε_{Nd} composition of northern
393 component deep water became less radiogenic, starting at about 4 to 3 Ma in the late
394 Neogene (Burton et al., 1997), and is now approximately -13.5 (Piepgras and
395 Wasserburg, 1987). Both of these changes are in a direction that makes it more
396 difficult to discern the influence of regional terrestrial sources from changes in
397 northern/southern component water mass mixing despite the higher Amazon
398 sediment fluxes. For example, a 60% contribution of Nd sourced from the Amazon
399 detrital sediments to Ceara Rise today ($\varepsilon_{\text{Nd}} = -10$; Allègre et al., 1996) would be
400 enough to increase the seawater value by 2 ε units above the modern northern
401 component water value. Such a change could be incorrectly interpreted to represent
402 an increased contribution from southern sourced deep waters at this site.

403 Authigenic ε_{Nd} records for the last 25 thousand years from piston cores GEO B1515-1
404 and GEOB 1523-1 on Ceara Rise (Figure 1) show a much more radiogenic signal
405 than we measure across the OMT, with values changing from about -10 at the last

406 glacial maximum to approximately -12 or -13 for the Holocene (Lippold et al.,
407 2016). This Pleistocene to Holocene shift is interpreted to be the result of a change in
408 water mass provenance at Ceara Rise, from predominantly Atlantic southern
409 component water to more unradiogenic northern component water (Lippold et al.,
410 2016). The Holocene Nd isotope compositions in these cores match modern seawater
411 ε_{Nd} (Piepgras and Wasserburg, 1987). We note however that these (de-)glacial deep
412 water ε_{Nd} values are close to modern Amazon suspended sediment values. Therefore,
413 a potential alternative explanation for these Pleistocene ε_{Nd} data could be a greater
414 influence of the benthic sedimentary flux of Nd ($\sim 60\%$ of total Nd) on deep water at
415 Ceara Rise during the last glacial maximum. This could be due to increased exposure
416 time to the benthic sedimentary Nd flux (e.g. Abbott et al., 2015a) during this time of
417 more sluggish Atlantic oceanic overturning (Lippold et al., 2016). Yet because both
418 an increased contribution of southern component water, and a higher flux of benthic
419 (pore fluid) Nd, act to shift deep water ε_{Nd} towards more radiogenic values, the effect
420 of enhanced Nd release from the particulate fraction at the last glacial maximum at
421 Ceara Rise cannot be unambiguously resolved at this stage.

422 **5 Conclusions**

423 We present ε_{Nd} records in fossilised fish teeth, planktonic foraminifera and Fe-Mn
424 oxyhydroxide substrates from Ceara Rise for the Oligocene-Miocene transition.
425 Records from these three substrates are remarkably consistent with one another,
426 implying that all three archives have acquired the ε_{Nd} signature of bottom waters. Yet
427 the ε_{Nd} data that we have obtained are extremely unradiogenic (down to -15) in
428 comparison to those for contemporaneous bottom waters in the Atlantic Ocean. They
429 cannot therefore be explained by simple large-scale ocean mixing between northern
430 and southern component Atlantic deep waters, both of which were significantly more
431 radiogenic (ε_{Nd} of -10 and -8 respectively). We suggest that bottom waters at Ceara
432 Rise were strongly influenced by inputs of Nd derived from weathering of ancient
433 cratonic rocks in the eastern Amazon drainage basin. The similarity between the fish
434 teeth, planktonic foraminifera, and Fe-Mn oxyhydroxide Nd isotope records provides
435 evidence for significant release of Nd from sedimentary particulate material from the

436 River Amazon during the OMT. Discovery of such a strong regional continental
437 influence on deep waters, many hundreds of kilometres from source, suggests that
438 boundary exchange processes can operate far from continental shelf regions (under
439 high particle flux conditions). Caution must therefore be exercised in site selection
440 and when interpreting seawater ϵ_{Nd} records in light of the vast distances across which
441 major point sources of Nd may influence deep water ϵ_{Nd} . On the other hand, these
442 techniques present an opportunity to investigate changes in sourcing of riverine-
443 supplied Nd to the ocean associated with major tectonic and/or climatic change.

444 **6 Acknowledgements**

445 This work used samples provided by the (Integrated) Ocean Drilling Program (ODP),
446 which is sponsored by the US National Science Foundation and participating
447 countries under management of the Joint Oceanographic Institutions (JOI), Inc. We
448 thank Walter Hale and staff at the Bremen Core Repository for their help in obtaining
449 core material and also Guy Rothwell of BOSCORF for providing core top material
450 for production of our in-house foraminiferal calcite standards. We thank Dieter
451 Garbe-Schönberg (University Kiel) and Ana Kolevica (GEOMAR Kiel) for their help
452 in detrital sample processing. We are indebted to Gavin Foster, Carrie Lear, Dan
453 Murphy, Fred Le Moigne, Helen Griffin and Anya Crocker for their advice and
454 helpful discussion of the manuscript. We also thank Derek Vance for assistance with
455 deconvolution of Nd isotope data and Matt Cooper, Darryl Green and Andy Milton
456 for their help with laboratory work. Three anonymous reviewers and the editor
457 provided constructive reviews that improved an earlier version of the manuscript.

458 Financial support was provided by the UK Natural Environment Research Council,
459 award # NE/D005108/1 to R.H.J and NE/K014137/1 and a Royal Society Research
460 Merit Award to P.A.W.

461

462

463

464

465

466

467

468

469

Figure 1: Location of ODP Leg 154 Site 926B Ceara Rise in relation to other deep water ε_{Nd} records across the Oligocene-Miocene transition discussed in this study. Fe-Mn crust ALV539, 2,665 m water depth (O'Nions et al., 1998), Fe-Mn crust ROM46, 3,350 m water depth (Frank et al., 2003), Fish tooth record from ODP Site 1090, 3,700 m water depth (Scher and Martin, 2008). Colours correspond to line/marker colours in Figure 2. Inset shows location of ODP Site 926B in relation to the Amazon River mouth and piston core sites on Ceara Rise, GEOB 1515-1 (3,129 m water depth) and GEOB 1523-1 (3,292 m water depth) used in the study by Lippold et al. (2016).

470

471

472

473

474

475

476

477

478

479

480

481

482

483

Figure 2: ε_{Nd} records across the Oligocene-Miocene transition at ODP Site 926. **A.** Benthic oxygen isotope record for this site (Pälike et al., 2006), **B.** ε_{Nd} values for fossilised fish teeth (green triangles), planktonic foraminifera *D. venezuelana* (blue circles) and *G. bulloides* (red circles), Fe/Mn oxyhydroxides (black diamonds), and the detrital fraction (squares). Deep water ε_{Nd} values for the South Atlantic (Scher and Martin, 2008), Equatorial Atlantic (Frank et al., 2003), and North Atlantic (O'Nions et al., 1998) at the OMT are also shown for comparison. Colour scale corresponds to that used in Figure 3 showing potential Amazon basin source rock ε_{Nd} ranges for Guiana Shield, Purus Arch and Phanerozoic sediments (Allègre et al., 1996). **C.** Estimated percentage of ε_{Nd} seawater signal at Ceara Rise coming from Amazon sources relative to northern component water during the OMT. Error bars represent the 2 standard error of each measurement. Magnetostratigraphic correlation from ODP Site 1090 in the South Atlantic (Billups et al., 2002; Channell et al., 2003).

484

485

486

487

488

489

490

Figure 3: Geology of the Amazon Basin. Star shows the position of ODP Site 926 on Ceara Rise. Panel A. Coloured squares (colour scale corresponds to that used in Figure 2) show ε_{Nd} values of modern suspended sediments in Amazon tributaries (Allègre et al., 1996). Shaded regions show basement lithology. Panel B. Amazon drainage during the Oligocene-Miocene. Black arrows and blue dashed line show, respectively, the inferred drainage pattern and catchment area at this time (Figueiredo et al., 2009; Shephard et al., 2010).

491

492

493

494

495

496

Table 1: ε_{Nd} measurements of detrital sediments and Fe/Mn oxyhydroxides from the Oligocene-Miocene transition of ODP Site 926. Ages are calculated using the age model of Pälike et al. (2006). $\varepsilon_{\text{Nd}}(0)$ denotes measured ε_{Nd} values, and $\varepsilon_{\text{Nd}}(t)$ values have been adjusted for ingrowth of ^{143}Nd since the Oligocene (assumption: initial $^{147}\text{Sm}/^{144}\text{Nd}$ ratio 0.1412 for detrital and Fe-Mn oxyhydroxide samples).

497

498

499

500

501

502

503

Table 2: ε_{Nd} measurements of fossilised fish teeth and planktonic foraminifera (*D. venezuelana* and *G. bulloides*) from the Oligocene-Miocene transition of ODP Site 926. Ages are calculated using the age model of Pälike et al. (2006). $\varepsilon_{\text{Nd}}(0)$ denotes measured ε_{Nd} values, and $\varepsilon_{\text{Nd}}(t)$ values have been adjusted for ingrowth of ^{143}Nd since the Oligocene (assumption: initial $^{147}\text{Sm}/^{144}\text{Nd}$ ratio 0.1286 for fish teeth and 0.1412 for foraminifera samples).

504

505 7 References

- 506 Abbott, A.N., Haley, B.A., McManus, J., 2015a. Bottoms up: Sedimentary control of the deep North
507 Pacific Ocean's ϵ Nd signature. *Geology* 43, 1035.
- 508 Abbott, A.N., Haley, B.A., McManus, J., Reimers, C.E., 2015b. The sedimentary flux of dissolved rare
509 earth elements to the ocean. *Geochimica et Cosmochimica Acta* 154, 186-200.
- 510 Allègre, C.J., Dupré, B., Négrel, P., Gaillardet, J., 1996. Sr-Nd-Pb isotope systematics in Amazon and
511 Congo River systems: constraints about erosion processes. *Chemical Geology* 131, 93-112.
- 512 Arbuszewski, J.A., deMenocal, P.B., Cleroux, C., Bradtmiller, L., Mix, A., 2013. Meridional shifts of
513 the Atlantic intertropical convergence zone since the Last Glacial Maximum. *Nature Geosci* 6, 959-
514 962.
- 515 Arsouze, T., Dutay, J.C., Lacan, F., Jeandel, C., 2009. Reconstructing the Nd oceanic cycle using a
516 coupled dynamical - biogeochemical model. *Biogeosciences* 6, 2829-2846.
- 517 Bayon, G., German, C.R., Burton, K.W., Nesbitt, R.W., Rogers, N., 2004. Sedimentary Fe-Mn
518 oxyhydroxides as paleoceanographic archives and the role of aeolian flux in regulating oceanic
519 dissolved REE. *Earth and Planetary Science Letters* 224, 477-492.
- 520 Billups, K., Channell, J.E.T., Zachos, J., 2002. Late Oligocene to early Miocene geochronology and
521 paleoceanography from the subantarctic South Atlantic. *Paleoceanography* 17, 1004.
- 522 Blaser, P., Lippold, J., Gutjahr, M., Frank, N., Link, J.M., Frank, M., 2016. Extracting foraminiferal
523 seawater Nd isotope signatures from bulk deep sea sediment by chemical leaching. *Chemical Geology*
524 439, 189-204.
- 525 Burton, K.W., Ling, H.-F., O'Nions, R.K., 1997. Closure of the Central American Isthmus and its
526 effect on deep-water formation in the North Atlantic. *Nature* 386, 382-385.
- 527 Campbell, K.E., Frailey, C.D., Romero-Pittman, L., 2006. The Pan-Amazonian Ucayali Peneplain, late
528 Neogene sedimentation in Amazonia, and the birth of the modern Amazon River system.
529 *Palaeogeography, Palaeoclimatology, Palaeoecology* 239, 166-219.
- 530 Carter, P., Vance, D., Hillenbrand, C.D., Smith, J.A., Shoosmith, D.R., 2012. The neodymium isotopic
531 composition of waters masses in the eastern Pacific sector of the Southern Ocean. *Geochimica et
532 Cosmochimica Acta* 79, 41-59.
- 533 Channell, J.E.T., Galeotti, S., Martin, E.E., Billups, K., Scher, H.D., Stoner, J.S., 2003. Eocene to
534 Miocene magnetostratigraphy, biostratigraphy, and chemostratigraphy at ODP Site 1090 (sub-
535 Antarctic South Atlantic). *Geological Society of America Bulletin* 115, 607-623.
- 536 Cunha, P.R.C., Gonzaga, F.G., Coutinho, L.F.C., Feijó, F.J., 1994. Bacia do Amazonas, Boletim de
537 Geociências da Petrobras. 8(1), pp. 47-55.
- 538 Dobson, D.M., Dickens, G.R., Rea, D.K., 2001. Terrigenous sediment on Ceara Rise: a Cenozoic
539 record of South American orogeny and erosion. *Palaeogeography, Palaeoclimatology, Palaeoecology*
540 165, 215-229.

Influence of the Amazon River on the Nd isotope composition of deep water in the western equatorial Atlantic during the Oligocene-Miocene transition

- 541 Eiras, J.F., Becker, C.R., Souza, E.M., Gonzaga, F.G., Silva, J.G.F., Daniel, L.M.F., Matsuda, N.S.,
542 Feijó, F.J., 1994. Bacia do Solimões, Boletim de Geociências da Petrobras. 8(1), pp. 17–22.
- 543 Elmore, A.C., Piotrowski, A.M., Wright, J.D., Scrivner, A.E., 2011. Testing the extraction of past
544 seawater Nd isotopic composition from North Atlantic deep sea sediments and foraminifera. *Geochem.*
545 *Geophys. Geosyst.* 12, Q09008.
- 546 Figueiredo, J., Hoorn, C., van der Ven, P., Soares, E., 2009. Late Miocene onset of the Amazon River
547 and the Amazon deep-sea fan: Evidence from the Foz do Amazonas Basin. *Geology* 37, 619–622.
- 548 Frank, M., van de Flierdt, T., Halliday, A.N., Kubik, P.W., Hattendorf, B., Gunther, D., 2003.
549 Evolution of deepwater mixing and weathering inputs in the central Atlantic Ocean over the past 33
550 Myr. *Paleoceanography* 18, 1091.
- 551 Gibbs, R.J., 1967. The Geochemistry of the Amazon River System: Part I. The Factors that Control the
552 Salinity and the Composition and Concentration of the Suspended Solids. *Geological Society of*
553 *America Bulletin* 78, 1203–1232.
- 554 Goldstein, S.J., Jacobsen, S.B., 1987. The Nd and Sr isotopic systematics of river-water dissolved
555 material: Implications for the sources of Nd and Sr in seawater. *Chemical Geology: Isotope*
556 *Geoscience section* 66, 245–272.
- 557 Goldstein, S.L., Hemming, S.R., 2003. Long-lived isotopic tracers in oceanography,
558 paleoceanography, and ice-sheet dynamics. *Treatise on geochemistry* 6, 453–489.
- 559 Gutjahr, M., Frank, M., Stirling, C.H., Klemm, V., van de Flierdt, T., Halliday, A.N., 2007. Reliable
560 extraction of a deepwater trace metal isotope signal from Fe-Mn oxyhydroxide coatings of marine
561 sediments. *Chemical Geology* 242, 351–370.
- 562 Jeandel, C., 1993. Concentration and isotopic composition of Nd in the South Atlantic Ocean. *Earth*
563 *and Planetary Science Letters* 117, 581–591.
- 564 Jeandel, C., Arsouze, T., Lacan, F., Téchiné, P., Dutay, J.C., 2007. Isotopic Nd compositions and
565 concentrations of the lithogenic inputs into the ocean: A compilation, with an emphasis on the
566 margins. *Chemical Geology* 239, 156–164.
- 567 Kraft, S., Frank, M., Hathorne, E.C., Weldeab, S., 2013. Assessment of seawater Nd isotope signatures
568 extracted from foraminiferal shells and authigenic phases of Gulf of Guinea sediments. *Geochimica et*
569 *Cosmochimica Acta* 121, 414–435.
- 570 Lacan, F., Jeandel, C., 2005a. Acquisition of the neodymium isotopic composition of the North
571 Atlantic Deep Water. *Geochem. Geophys. Geosyst.* 6, Q12008.
- 572 Lacan, F., Jeandel, C., 2005b. Neodymium isotopes as a new tool for quantifying exchange fluxes at
573 the continent-ocean interface. *Earth and Planetary Science Letters* 232, 245–257.
- 574 Liebrand, D., Lourens, L.J., Hodell, D.A., de Boer, B., van de Wal, R.S.W., Pälike, H., 2011. Antarctic
575 ice sheet and oceanographic response to eccentricity forcing during the early Miocene. *Climate of the*
576 *Past* 7, 869–880.
- 577 Lippold, J., Gutjahr, M., Blaser, P., Christner, E., de Carvalho Ferreira, M.L., Mulitza, S., Christl, M.,
578 Wombacher, F., Böhm, E., Antz, B., Cartapanis, O., Vogel, H., Jaccard, S.L., 2016. Deep water
579 provenance and dynamics of the (de)glacial Atlantic meridional overturning circulation. *Earth and*
580 *Planetary Science Letters* 445, 68–78.

- 581 Martin, E.E., Haley, B.A., 2000. Fossil fish teeth as proxies for seawater Sr and Nd isotopes. Geochimica et Cosmochimica Acta 64, 835-847.
- 583 Martin, E.E., Scher, H.D., 2004. Preservation of seawater Sr and Nd isotopes in fossil fish teeth: bad
584 news and good news. Earth and Planetary Science Letters 220, 25-39.
- 585 McDaniel, D.K., McLennan, S.M., Hanson, G.N., 1997. Provenance of Amazon Fan muds: constraints
586 from Nd and Pb isotopes, in: Flood, R.D., Piper, D.J.W., Klaus, A., Peterson, L.C. (Eds.), Proceedings
587 of the Ocean Drilling Program, Scientific Results, pp. 155: 169-176.
- 588 O'Nions, R.K., Frank, M., von Blanckenburg, F., Ling, H.F., 1998. Secular variation of Nd and Pb
589 isotopes in ferromanganese crusts from the Atlantic, Indian and Pacific Oceans. Earth and Planetary
590 Science Letters 155, 15-28.
- 591 Osborne, A.H., Haley, B.A., Hathorne, E.C., Flögel, S., Frank, M., 2014. Neodymium isotopes and
592 concentrations in Caribbean seawater: Tracing water mass mixing and continental input in a semi-
593 enclosed ocean basin. Earth and Planetary Science Letters 406, 174-186.
- 594 Pälike, H., Frazier, J., Zachos, J.C., 2006. Extended orbitally forced palaeoclimatic records from the
595 equatorial Atlantic Ceara Rise. Quat. Sci. Rev. 25, 3138-3149.
- 596 Pearce, C.R., Jones, M.T., Oelkers, E.H., Pradoux, C., Jeandel, C., 2013. The effect of particulate
597 dissolution on the neodymium (Nd) isotope and Rare Earth Element (REE) composition of seawater.
598 Earth and Planetary Science Letters 369-370, 138-147.
- 599 Piepras, D.J., Wasserburg, G.J., 1987. Rare earth element transport in the western North Atlantic
600 inferred from Nd isotopic observations. Geochimica et Cosmochimica Acta 51, 1257-1271.
- 601 Piotrowski, A.M., Goldstein, S.L., Hemming, S.R., Fairbanks, R.G., 2005. Temporal Relationships of
602 Carbon Cycling and Ocean Circulation at Glacial Boundaries. Science 307, 1933-1938.
- 603 Pomiès, C., Davies, G.R., Conan, S.M.H., 2002. Neodymium in modern foraminifera from the Indian
604 Ocean: implications for the use of foraminiferal Nd isotope compositions in paleo-oceanography.
605 Earth and Planetary Science Letters 203, 1031-1045.
- 606 Rempfer, J., Stocker, T.F., Joos, F., Dutay, J.-C., Siddall, M., 2011. Modelling Nd-isotopes with a
607 coarse resolution ocean circulation model: Sensitivities to model parameters and source/sink
608 distributions. Geochimica et Cosmochimica Acta 75, 5927-5950.
- 609 Roberts, N.L., Piotrowski, A.M., Elderfield, H., Eglinton, T.I., Lomas, M.W., 2012. Rare earth
610 element association with foraminifera. Geochimica et Cosmochimica Acta 94, 57-71.
- 611 Rosenthal, Y., Field, M.P., Sherrell, R.M., 1999. Precise determination of element/calcium ratios in
612 calcareous samples using sector field inductively coupled plasma mass spectrometry. Anal. Chem. 71,
613 3248-3253.
- 614 Rousseau, T.C.C., Sonke, J.E., Chmeleff, J., van Beek, P., Souhaut, M., Boaventura, G., Seyler, P.,
615 Jeandel, C., 2015. Rapid neodymium release to marine waters from lithogenic sediments in the
616 Amazon estuary. Nat Commun 6.
- 617 Scher, H.D., Martin, E.E., 2004. Circulation in the Southern Ocean during the Paleogene inferred from
618 neodymium isotopes. Earth and Planetary Science Letters 228, 391-405.

Influence of the Amazon River on the Nd isotope composition of deep water in the western equatorial Atlantic during the Oligocene-Miocene transition

- 619 Scher, H.D., Martin, E.E., 2008. Oligocene deep water export from the North Atlantic and the
620 development of the Antarctic Circumpolar Current examined with neodymium isotopes.
621 Paleoceanography 23, PA1205.
- 622 Scher, H.D., Martin, E.E., 2006. Timing and Climatic Consequences of the Opening of Drake Passage.
623 Science 312, 428-430.
- 624 Shephard, G.E., Muller, R.D., Liu, L., Gurnis, M., 2010. Miocene drainage reversal of the Amazon
625 River driven by plate-mantle interaction. Nature Geoscience 3, 870-875.
- 626 Shipboard Scientific Party, 1995. Site 926, in: Curry, W.B., Shackleton, N.J., Richter, C., et al., (Ed.),
627 Proceedings of the Ocean Drilling Program. Initial Reports. College Station, TX (Ocean Drilling
628 Program), pp. 154: 153-232.
- 629 Stewart, J.A., Wilson, P.A., Edgar, K.M., Anand, P., James, R.H., 2012. Geochemical assessment of
630 the palaeoecology, ontogeny, morphotypic variability and palaeoceanographic utility of
631 "Dentoglobigerina" venezuelana. Marine Micropaleontology 84-85, 74-86.
- 632 Stichel, T., Frank, M., Rickli, J., Haley, B.A., 2012. The hafnium and neodymium isotope composition
633 of seawater in the Atlantic sector of the Southern Ocean. Earth and Planetary Science Letters
634 317, Äi318, 282-294.
- 635 Tachikawa, K., Athias, V., Jeandel, C., 2003. Neodymium budget in the modern ocean and paleo-
636 oceanographic implications. Journal of Geophysical Research 108, 3254.
- 637 Tachikawa, K., Piotrowski, A.M., Bayon, G., 2014. Neodymium associated with foraminiferal
638 carbonate as a recorder of seawater isotopic signatures. Quat. Sci. Rev. 88, 1-13.
- 639 Tanaka, T., Togashi, S., Kamioka, H., Amakawa, H., Kagami, H., Hamamoto, T., Yuhara, M.,
640 Orihashi, Y., Yoneda, S., Shimizu, H., Kunimaru, T., Takahashi, K., Yanagi, T., Nakano, T., Fujimaki,
641 H., Shinjo, R., Asahara, Y., Tanimizu, M., Dragusanu, C., 2000. JNdi-1: a neodymium isotopic
642 reference in consistency with LaJolla neodymium. Chemical Geology 168, 279-281.
- 643 Thomas, D.J., Bralower, T.J., Jones, C.E., 2003. Neodymium isotopic reconstruction of late Paleocene
644 - early Eocene thermohaline circulation. Earth and Planetary Science Letters 209, 309-322.
- 645 van der Hammen, T., Hooghiemstra, H., 2000. Neogene and Quaternary history of vegetation, climate,
646 and plant diversity in Amazonia. Quat. Sci. Rev. 19, 725-742.
- 647 Vance, D., Burton, K., 1999. Neodymium isotopes in planktonic foraminifera: a record of the response
648 of continental weathering and ocean circulation rates to climate change. Earth and Planetary Science
649 Letters 173, 365-379.
- 650 Vance, D., Scrivner, A.E., Beney, P., Staubwasser, M., Henderson, G.M., Slowey, N.C., 2004. The use
651 of foraminifera as a record of the past neodymium isotope composition of seawater. Paleoceanography
652 19, PA2009.
- 653 Vance, D., Thirlwall, M., 2002. An assessment of mass discrimination in MC-ICPMS using Nd
654 isotopes. Chemical Geology 185, 227-240.
- 655 Wang, X., Auler, A.S., Edwards, R.L., Cheng, H., Cristalli, P.S., Smart, P.L., Richards, D.A., Shen,
656 C.-C., 2004. Wet periods in northeastern Brazil over the past 210 kyr linked to distant climate
657 anomalies. Nature 432, 740-743.

Influence of the Amazon River on the Nd isotope composition of deep water in the western equatorial Atlantic during the
Oligocene-Miocene transition

- 658 West, A.J., Galy, A., Bickle, M., 2005. Tectonic and climatic controls on silicate weathering. Earth
659 and Planetary Science Letters 235, 211-228.
- 660 Wilson, D.J., Piotrowski, A.M., Galy, A., McCave, I.N., 2012. A boundary exchange influence on
661 deglacial neodymium isotope records from the deep western Indian Ocean. Earth and Planetary
662 Science Letters 341-344, 35-47.
- 663 Wombacher, F., Rehkämper, M., 2003. Investigation of the mass discrimination of multiple collector
664 ICP-MS using neodymium isotopes and the generalised power law. Journal of Analytical Atomic
665 Spectrometry 18.
- 666

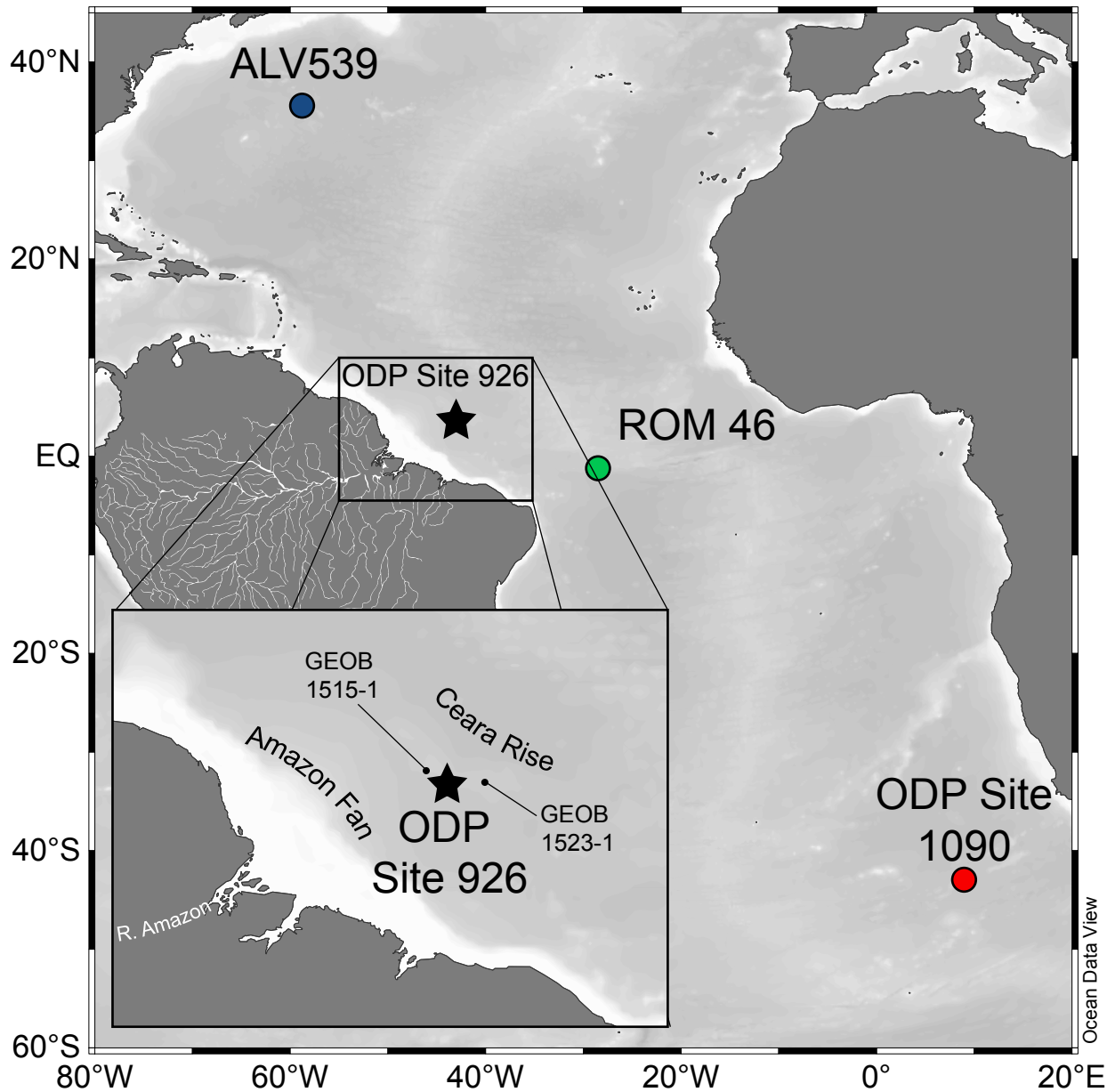


Figure 1: Location of ODP Leg 154 Site 926B Ceara Rise in relation to other deep water ϵ Nd records across the Oligocene-Miocene transition discussed in this study. Fe-Mn crust ALV539, 2,665 m water depth (O'Nions et al., 1998), Fe-Mn crust ROM46, 3,350 m water depth (Frank et al., 2003), Fish tooth record from ODP Site 1090, 3,700 m water depth (Scher and Martin, 2008). Colours correspond to line/marker colours in Figure 2. Inset shows location of ODP Site 926B in relation to the Amazon River mouth and piston core sites on Ceara Rise, GEOB 1515-1 (3,129 m water depth) and GEOB 1523-1 (3,292 m water depth) used in the study by Lippold et al. (2016).

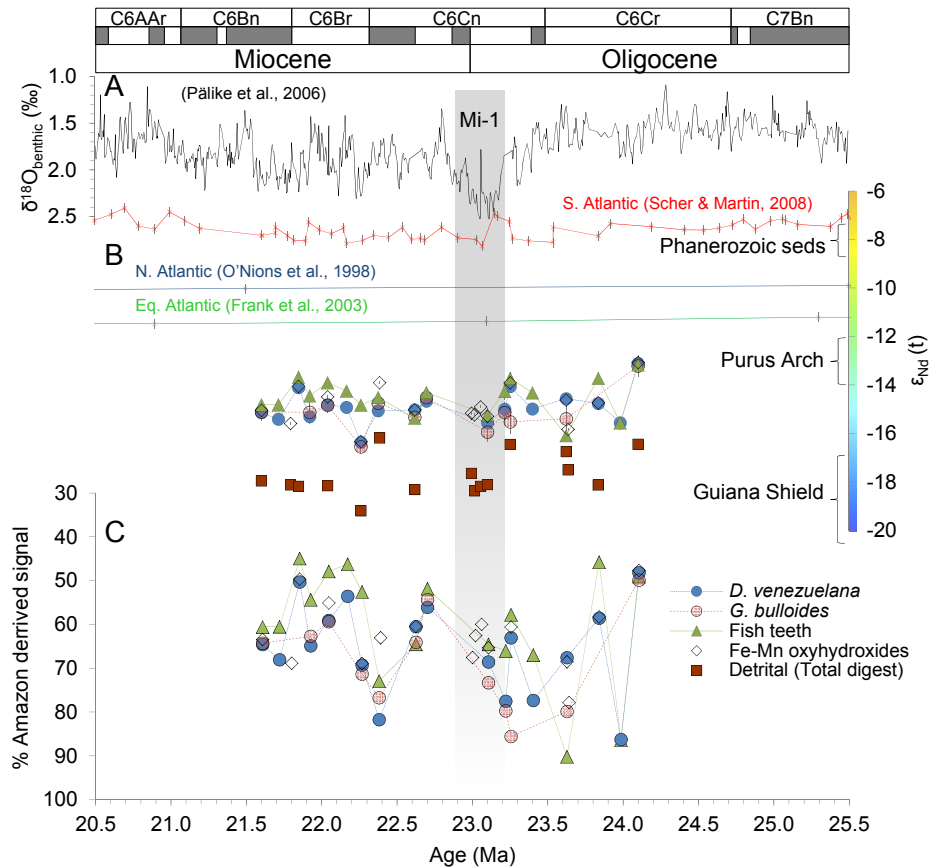


Figure 2: ϵ_{Nd} records across the Oligocene-Miocene transition at ODP Site 926. A. Benthic oxygen isotope record for this site (Pälike et al., 2006), B. ϵ_{Nd} values for fossilised fish teeth (green triangles), planktonic foraminifera *D. venezuelana* (blue circles) and *G. bulloides* (red circles), Fe/Mn oxyhydroxides (black diamonds), and the detrital fraction (squares). Deep water ϵ_{Nd} values for the South Atlantic (Scher and Martin, 2008), Equatorial Atlantic (Frank et al., 2003), and North Atlantic (O'Nions et al., 1998) at the OMT are also shown for comparison. Colour scale corresponds that used in Figure 3 showing potential Amazon basin source rock ϵ_{Nd} ranges for Guiana Shield, Purus Arch and Phanerozoic sediments (Allègre et al., 1996). C. Estimated percentage of ϵ_{Nd} seawater signal at Ceara Rise coming from Amazon sources relative to northern component water during the OMT. Error bars represent the 2 standard error of each measurement. Magnetostratigraphic correlation from ODP Site 1090 in the South Atlantic (Billups et al., 2002; Channell et al., 2003).

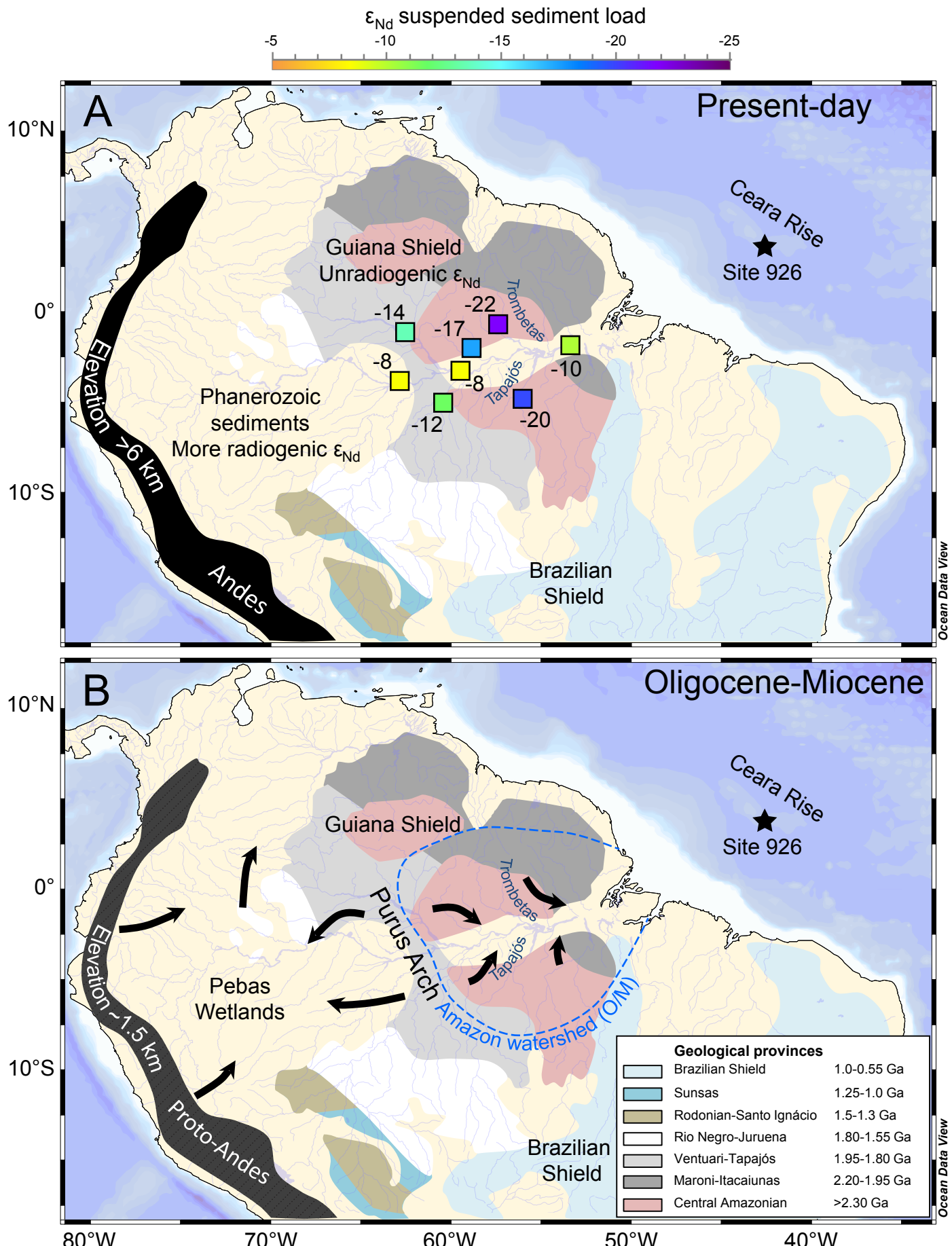


Figure 3: Geology of the Amazon Basin. Star shows the position of ODP Site 926 on Ceará Rise. Panel A. Coloured squares (colour scale corresponds to that used in Figure 2) show ϵ_{Nd} values of modern suspended sediments in Amazon tributaries (Allègre et al., 1996). Shaded regions show basement lithology. Panel B. Amazon drainage during the Oligocene-Miocene. Black arrows and blue dashed line show, respectively, the inferred drainage pattern and catchment area at this time (Figueiredo et al., 2009; Shephard et al., 2010).

ODP Sample Identification				Depth (mbsf)	Age (Ma)	Detrital (Total digest)			Fe-Mn oxyhydroxides				
Site, Hole, Core, Section,	Half, Int.					$^{143}\text{Nd}/^{144}\text{Nd}$ (normalised)	$\varepsilon_{\text{Nd}}(0)$	$\varepsilon_{\text{Nd}}(t)$	$^{143}\text{Nd}/^{144}\text{Nd}$ (normalised)	$\varepsilon_{\text{Nd}}(0)$	$\varepsilon_{\text{Nd}}(t)$		
						2SE		2SE		2SE			
926 B	46	4 W	40 - 50	427.8	21.61	0.511710	-18.10	-17.95	0.06	0.511859	-15.20	-15.04	0.05
926 B	46	6 W	70 - 80	431.1	21.72								
926 B	47	1 W	65 - 67	433.1	21.80	0.511701	-18.27	-18.12	0.05	0.511831	-15.74	-15.59	0.06
926 B	47	2 W	70 - 80	434.7	21.85	0.511698	-18.33	-18.17	0.05	0.511909	-14.21	-14.06	0.08
926 B	47	4 W	10 - 20	437.1	21.93								
926 B	47	6 W	42 - 50	440.4	22.05	0.511700	-18.30	-18.15	0.06	0.511887	-14.64	-14.49	0.06
926 B	48	2 W	72 - 80	444.4	22.17								
926 B	48	4 W	52 - 60	447.2	22.27	0.511647	-19.34	-19.18	0.05	0.511793	-16.49	-16.33	0.05
926 B	48	6 W	91 - 100	450.6	22.38								
926 B	48	6 W	132 - 134	450.9	22.39	0.511800	-16.34	-16.19	0.05	0.511917	-14.06	-13.90	0.06
926 B	49	4 W	109 - 120	457.3	22.62	0.511691	-18.47	-18.31	0.05	0.511860	-15.18	-15.02	0.04
926 B	49	6 W	5 - 15	459.3	22.70								
926 B	50	4 W	102 - 105	466.9	23.00	0.511725	-17.81	-17.64	0.04	0.511852	-15.32	-15.16	0.05
926 B	50	5 W	5.5 - 7.5	467.5	23.02	0.511688	-18.52	-18.36	0.05	0.511849	-15.39	-15.23	0.05
926 B	50	5 W	111 - 114	468.5	23.06	0.511698	-18.34	-18.18	0.05	0.511866	-15.07	-14.90	0.04
926 B	50	6 W	82 - 92	469.8	23.11	0.511702	-18.27	-18.10	0.04	0.511846	-15.45	-15.29	0.05
926 B	51	2 W	35 - 45	472.9	23.22								
926 B	51	2 W	128 - 133	473.8	23.26	0.511786	-16.61	-16.45	0.05	0.511917	-14.07	-13.91	0.06
926 B	51	5 W	53 - 60	477.6	23.40								
926 B	52	1 W	94 - 104	481.5	23.63	0.511771	-16.91	-16.75	0.06	0.511880	-14.79	-14.62	0.06
926 B	52	1 W	141 - 143	481.9	23.64	0.511733	-17.66	-17.49	0.05	0.511818	-16.00	-15.83	0.05
926 B	52	5 W	29 - 38	486.8	23.84	0.511700	-18.29	-18.12	0.05	0.511874	-14.90	-14.73	0.05
926 B	53	1 W	35 - 44	490.6	23.99								
926 B	53	3 W	105 - 114	494.3	24.10	0.511786	-16.62	-16.44	0.04	0.511959	-13.24	-13.07	0.05

Table 1: ε_{Nd} measurements of detrital sediments and Fe/Mn oxyhydroxides from the Oligocene-Miocene transition of ODP Site 926. Ages are calculated using the age model of Pälike et al. (2006). $\varepsilon_{\text{Nd}}(0)$ denotes measured ε_{Nd} values, and $\varepsilon_{\text{Nd}}(t)$ values have been adjusted for ingrowth of ^{143}Nd since the Oligocene (assumption: initial $^{147}\text{Sm}/^{144}\text{Nd}$ ratio 0.1412 for detrital and Fe-Mn oxyhydroxide samples).

ODP Sample Identification Site, Hole, Core, Section, Half, Int.	Depth (mbsf)	Age (Ma)	Fish teeth		<i>D. venezuelana</i>		<i>G. bulloides</i>								
			$^{143}\text{Nd}/^{144}\text{Nd}$ (normalised)	$\varepsilon_{\text{Nd}}(0)$	$\varepsilon_{\text{Nd}}(t)$	$^{143}\text{Nd}/^{144}\text{Nd}$ (normalised)	$\varepsilon_{\text{Nd}}(0)$	$\varepsilon_{\text{Nd}}(t)$	$^{143}\text{Nd}/^{144}\text{Nd}$ (normalised)						
					2SE		2SE		2SE						
926 B 46 4 W	40 - 50	427.8	21.61	0.511869	-15.00	-14.81	0.19	0.511854	-15.28	-15.13	0.22	0.511856	-15.26	-15.11	0.39
926 B 46 6 W	70 - 80	431.1	21.72	0.511869	-15.00	-14.81	0.18	0.511840	-15.56	-15.41	0.20				
926 B 47 1 W	65 - 67	433.1	21.80												
926 B 47 2 W	70 - 80	434.7	21.85	0.511928	-13.86	-13.67	0.17	0.511907	-14.26	-14.11	0.21				
926 B 47 4 W	10 - 20	437.1	21.93	0.511888	-14.63	-14.44	0.19	0.511846	-15.45	-15.30	0.23	0.511855	-15.27	-15.12	0.46
926 B 47 6 W	42 - 50	440.4	22.05	0.511916	-14.09	-13.90	0.19	0.511871	-14.96	-14.81	0.20	0.511870	-14.99	-14.83	0.31
926 B 48 2 W	72 - 80	444.2	22.17	0.511898	-14.43	-14.25	0.18	0.511865	-15.07	-14.92	0.27				
926 B 48 4 W	52 - 60	447.2	22.27	0.511868	-15.02	-14.83	0.19	0.511791	-16.52	-16.36	0.17	0.511782	-16.70	-16.55	0.25
926 B 48 6 W	91 - 100	450.6	22.38	0.511884	-14.70	-14.51	0.18	0.511858	-15.21	-15.06	0.23	0.511874	-14.90	-14.75	0.24
926 B 48 6 W	132 - 134	450.9	22.39												
926 B 49 4 W	109 - 120	457.3	22.62	0.511841	-15.56	-15.36	0.18	0.511860	-15.18	-15.03	0.16	0.511844	-15.48	-15.32	0.27
926 B 49 6 W	5 - 15	459.3	22.70	0.511895	-14.50	-14.31	0.20	0.511878	-14.82	-14.66	0.20	0.511886	-14.67	-14.51	0.19
926 B 50 4 W	102 - 105	466.9	23.00												
926 B 50 5 W	5.5 - 7.5	467.5	23.02												
926 B 50 5 W	111 - 114	468.5	23.06												
926 B 50 6 W	82 - 92	469.8	23.11	0.511847	-15.43	-15.23	0.26	0.511832	-15.72	-15.56	0.20	0.511813	-16.10	-15.94	0.40
926 B 51 2 W	35 - 45	472.9	23.22	0.511897	-14.46	-14.26	0.36	0.511861	-15.16	-15.00	0.25	0.511854	-15.30	-15.14	0.43
926 B 51 2 W	128 - 133	473.8	23.26	0.511924	-13.92	-13.72	0.24	0.511909	-14.23	-14.06	0.22	0.511834	-15.68	-15.52	0.50
926 B 51 5 W	53 - 60	477.6	23.40	0.511894	-14.52	-14.32	0.20	0.511861	-15.15	-14.99	0.24				
926 B 52 1 W	94 - 104	481.5	23.63	0.511803	-16.29	-16.09	0.16	0.511883	-14.72	-14.56	0.18	0.511841	-15.55	-15.39	0.71
926 B 52 1 W	141 - 143	481.9	23.64												
926 B 52 5 W	29 - 38	486.8	23.84	0.511924	-13.92	-13.72	0.25	0.511873	-14.92	-14.76	0.21				
926 B 53 1 W	35 - 44	490.6	23.99	0.511830	-15.77	-15.57	0.19	0.511832	-15.72	-15.56	0.24				
926 B 53 3 W	105 - 114	494.3	24.10	0.511953	-13.37	-13.16	0.26	0.511958	-13.27	-13.11	0.21	0.511952	-13.38	-13.21	0.45

Table 2: ε_{Nd} measurements of fossilised fish teeth and planktonic foraminifera (*D. venezuelana* and *G. bulloides*) from the Oligocene-Miocene transition of ODP Site 926. Ages are calculated using the age model of Pälike et al. (2006). $\varepsilon_{\text{Nd}}(0)$ denotes measured ε_{Nd} values, and $\varepsilon_{\text{Nd}}(t)$ values have been adjusted for ingrowth of ^{143}Nd since the Oligocene (assumption: initial $^{147}\text{Sm}/^{144}\text{Nd}$ ratio 0.1286 for fish teeth and 0.1412 for foraminifera samples).